Journal of Materials Chemistry

Cite this: *J. Mater. Chem.*, 2011, **21**, 14213

www.rsc.org/materials

PAPER

Formation of hierarchical silica nanochannels through nanoimprint lithography†

Nicholas R. Hendricks, James J. Watkins* and Kenneth R. Carter*

Received 8th April 2011, Accepted 1st July 2011
DOI: 10.1039/c1jm11493j

Hierarchically structured silica nanochannels were fabricated through the combination of supercritical carbon dioxide mediated silica deposition and nanoimprint lithography of a sacrificial polymer template. Highly-ordered mesoporous silica was prepared with either spherical or cylindrical domain level features, ~5–6 nm in diameter, to compliment the device level structure of the embedded nanochannels. The hierarchical structure was used as a test device for low-k dielectric materials with a dielectric constant of 2.0 observed.

Introduction

The fabrication of mesoporous silica nanochannels with hierarchical structure has attracted increasing interest for applications such as ultra-low-k dielectric materials for microelectronics,[1–3] separations media, catalyst substrates,[4,5] chemical sensors,[6,7] and micro/nanofluidic devices.[8] These applications benefit from the hierarchical structures, which exhibit features at two distinct length scales. At the domain level, the films contain well defined pores, generally of discrete size distributions with diameters in the range of 3 to 10 nm, although larger pores are possible. At the device level, channel structures on the order of 25 to 500 nm provide increased porosity and fluid flow capabilities. Several approaches have previously been taken to create embedded nanochannels. These include the combinations of electron-beam (e-beam) lithography, reactive ion etching (RIE), wet etching,[9,10] or focused-ion beam (FIB) milling techniques to create the template and channel isolation with wafer bonding procedures, sacrificial material templates,[11] directed self assembly of nanoparticles,[12] nanoimprint lithography,[13–16] buried channel technology,[17] and surface nanomachining.[18]

Of particular interest to the semiconductor community is the formation of air-gap structures for use as an ultra-low-k (ULK) interlayer dielectric (ILD). As the size of interconnects continues to decrease, the capacitance that resides between metallic interconnects continues to increase. The objective is to diminish the capacitance between interconnects for decreased resistive-capacitive (RC) delay and reduced power consumption. The materials approach to reduce the dielectric constant of ILDs is to incorporate air into the ILD, by either porosity or air-gaps, effectively replacing a higher dielectric constant materials, for example, silicon dioxide with a dielectric constant of ~3.9, with air, which has a dielectric constant of ~1. Popular methods to create air-gaps are through sacrificial material removal and non-conformal chemical vapor deposition (CVD).[19–21] Here we report an alternative, efficient route for the fabrication of embedded nanochannels within a mesoporous film that involves a combination of supercritical carbon dioxide ($scCO_2$) infusion with nanoimprint lithography (NIL). The combination of these two techniques enables precise design of both domain and device level structures.

To produce well-ordered mesoporous silica films, Watkins *et al.* have reported the three-dimensional (3-D) replication of phase separated block copolymer templates in $scCO_2$.[22] The block copolymer thin film templates are prepared by spin-coating amphiphilic block copolymer solutions with hydrophilic homopolymers and catalytic amounts of organic acid. The amphiphilic block copolymer template is then exposed to a humidified $scCO_2$ solution of a silica precursor such as silicon alkoxides. During phase separation of the template, the organic acid partitions towards the hydrophilic domains of the template such that upon introduction of $scCO_2$, hydrolysis and condensation of the precursor to form the silica network occurs exclusively within the hydrophilic domains of the template. The unmodified hydrophobic domains of the template subsequently play the role of the porogen, *i.e.* the chemistry is phase selective. Only within the presence of the acid catalyst will the silicon alkoxide hydrolyze and condense to form the silica network. The use of $scCO_2$ allows for the amphiphilic block copolymer template to be dilated sufficiently, permitting uniform infiltration of the silica precursors within the template to provide a high fidelity silica template replication. The infused silica/block copolymer composite is then subjected to a 400 °C calcination to remove the polymer template to yield a mesoporous silica thin film. Through this $scCO_2$ infusion process of silicon alkoxide precursors into a block copolymer template, the size and shape of the domain level

Polymer Science and Engineering Department, University of Massachusetts Amherst, Conte Center for Polymer Research, 120 Governors Drive, Amherst, MA, 01003, USA. E-mail: krcarter@polysci.umass.edu; watkins@polysci.umass.edu

† Electronic supplementary information (ESI) available. See DOI: 10.1039/c1jm11493j

structure of the hierarchical nanochannels can be easily modified by changing the block copolymer molecular weight or by changing individual block lengths.[23] The $scCO_2$ infusion process also separates the ordering of the block copolymer template from the inorganic matrix formation to allow adjustments to be made to the template before the metal oxide network is established. In addition, the use of block copolymer templates that can be lithographically patterned *via* chemical amplification in the presence of photo-acid generators upon exposure to ultraviolet (UV) light provides a means of simultaneously imparting mesoporosity and 2-D device level surface patterning.[24,25]

To enable the fabrication of novel 3-D device level features of the hierarchical structure, specifically buried nanochannels, the use of NIL to create sacrificial templates is employed. Imprint lithography has garnered tremendous interest from the lithography community since the first reported use of this technique in 1995 due to the simplicity of the process, high throughput, high resolution and low cost.[26] Two general methods of NIL are widely used to produce nanoscopic features. The first involves thermal imprinting into a thermoplastic material at elevated temperatures and pressures.[26,27] The second is a UV assisted NIL in which resist materials are comprised of UV curable monomers and undergo chemical crosslinking upon exposure to UV radiation.[28,29]

The fabrication of hierarchical structure silica nanochannels having domain level porosity from the $scCO_2$ infusion process and device level porosity from NIL generated sacrificial templates is reported. The combination of $scCO_2$ infusion and NIL has allowed for the fabrication of hierarchical silica nanochannels with designable and adjustable porosity for microelectronic, micro/nanofluidic, chemical sensor and separation applications.

Experimental

Materials

3-(Trimethoxysilyl)propyl methacrylate (98%, Aldrich), ethoxylated-bisphenol A dimethacrylate esters (Sartomer), trimethylolpropane triacrylate (tech., Aldrich), propylene glycol methyl ether acetate (≥99.5%, Aldrich), Pluronic® F127 and Pluronic® F108 block copolymers (BASF), *para*-toluene sulfonic acid (99%, Acros Organics), poly(acrylic acid) (1.8k MW, Aldrich) and tetraethyl orthosilicate (99.999%, Sigma-Aldrich) were used as received without further purification. Silicon wafers of (100) orientation (p-type, boron dopant) were obtained from University Wafer.

Silicon wafer preparation

Silicon substrates (1″ × 1″) were coated with a self-assembled monolayer (SAM) of 3-(trimethoxysilyl)propyl methacrylate that is anchored to a silicon substrate and serves as an adhesion promoter. The silicon wafer surface must be modified with an adhesion promoter to adjust the surface energies of the substrate to be compatible with the UV curable resist, which allows a uniform, thin film to be spin-coated. The silicon wafer pieces were rinsed with acetone and isopropanol (IPA), dried under a stream of nitrogen (N_2) and then etched with an oxygen (O_2) plasma with an inductively coupled plasma (ICP) etcher (30 W, 100 mTorr) for 15 min to remove any surface contamination. The silicon wafers were then rinsed with water and ethanol, dried under a stream of N_2 and immediately placed in a 1 vol. % solution of 3-(trimethoxysilyl)propyl methacrylate in dry toluene at 80 °C for 2 h. Upon removal from the adhesion promotion solution, the silicon wafers were rinsed with IPA and dried under a stream of N_2. A static water contact angle measurement of 81 ± 2° is reported for the 3-(trimethoxysilyl)propyl methacrylate SAM surface.

Nanoimprint lithography

A UV curable photopolymer solution comprised of ethoxylated-bisphenol A dimethacrylate, trimethylolpropane triacrylate and 2,2-dimethoxy-2-phenylacetophenone dissolved in propylene glycol methyl ether acetate (PGMEA) was spin-coated at 3000 rpm for 15 s on the adhesion promoted substrate. The concentration of the photoresist solution determined the film thickness with typical concentrations ranging from 1 wt.% to 20 wt.% which yield film thicknesses from ~25 nm to ~400 nm. Thin films of the UV curable photoresist were patterned with transparent, fluorinated molds (for a detailed description of the mold fabrication, see Supporting Information, Schemes S1 and S2) using a Nanonex NX-2000 Nanoimprinter tool with the following conditions: the pre-imprint was made at 25 °C and 0.86 MPa (125 PSI) for 30 s, the imprint was made at 25 °C and 1.38 MPa (200 PSI) for 60 s with the last 30 s of the imprint time irradiating the sample with 365 nm UV light from a Dymax Bluewave® 200 UV light source (upon exposure to 365 nm UV light, the UV curable resist undergoes a crosslinking polymerization) and then the pressure was released. The fluorinated mold and sample was then manually separated by assistance of a razor blade and compressed air.

Anisotropic etching

Following NIL replication, the thin residual layer, approximately 10–15 nm in thickness, connecting the features was removed using dry etching. An inductively coupled plasma reactive ion etch (ICP-RIE) with O_2 plasma (150 W ICP, 30 W RIE, 250 mTorr, 49 sccm O_2) was applied for 30 s and resulted in free-standing structures.

Supercritical carbon dioxide infusion process

Mesoporous silica films were generated by exposing amphiphilic block copolymer templates to a solution of tetraethyl orthosilicate (TEOS) in $scCO_2$ within a high pressure reactor at 60 °C and 125 bar. The high pressure reactor, ~160 mL in volume, is constructed from two stainless steel opposed ended hubs sealed with a graphite ring (55 ft-lb torque) purchased from Grayloc® Products. Heating bands (Watlow®) are connected to the outside of the reactor walls to control the gas temperature. The top reactor hub is drilled to have 4 ports; one to measure internal pressure, one to measure internal temperature, one for gas inlet and one for gas outlet.

For the Pluronic® surfactant solutions (Pluronic® F127 or Pluronic® F108) containing 40 wt.% poly(acrylic acid) (PAA, 1.8k Mw, with respect to Pluronic F127® or Pluronic F108®) and 3 wt.% pTSA (with respect to solid material), TEOS

(6–10 μL) was directly placed within the high pressure reactor along with 500 μL of reverse osmosis (RO) water prior to sealing. Once the reactor was sealed and heated to a gas temperature of 60 °C, the carbon dioxide (CO_2, Merriam Graves, bone-dry grade) was injected with a high pressure syringe pump (ISCO, Model 500 HP) at a rate of 2–3 mL/min. Once the correct pressure was reached, a soak time of 2 h at 60 °C and 125 bar was observed. The reactor was then de-pressurized overnight to room pressure. Samples were thermally degraded at 400 °C for 6 h with a ramp rate of 1.56 °C min^{-1} in an air environment.

Capacitance measurements

The hierarchically structured silica nanochannels were fabricated on low-resistivity silicon wafers (0.001–0.005 Ω cm, University Wafers) to minimize the capacitance associated with the silicon wafer. The samples were directly taken from the thermal degradation oven to a 150 °C pre-heated hexamethyldisilazane (HMDS) vapor prime oven (YES LP-III vapor prime oven) for hydrophobic treatment. This was done to minimize the uptake of atmospheric water by the mesoporous silica. The top contact for the capacitance measurements was performed by deposition of ~100 nm of aluminum (99.999%, Ted Pella, Inc.) by electron-beam evaporation (CHA SE-600 electron beam evaporator) using a shadow mask consisting of 1 mm, 1.5 mm, and 2 mm diameter pads. Capacitance measurements were conducted with a Keithley 4200 Semiconductor Characterization System using a Wentworth MP-2300 probe station. A frequency of 100 kHz was used with a sweep voltage from 0 V to −5 V using a step size of 0.1 V.

Characterization

Water contact angle measurements were conducted using a VCA Optima surface analysis/goniometry system with a 0.5 μL drop. Atomic force microscopy (AFM) images were collected with a Digital Instruments Nanoscope IIIA in tapping mode under ambient conditions. Thermogravimetric analysis (TGA) was conducted with a DuPont TGA 2950 using a ramp rate of 1.56 °C min^{-1} and holding at 400 °C for 6 h under an air environment. Attenuated total reflectance Fourier transform infrared (ATR-FT-IR) measurements were collected on a Nicolet 6700 FT-IR spectrometer equipped with a Harrick grazing angle ATR accessory (GATR) with a liquid N_2 cooled photovoltaic detector (LN-MCT). Sample preparation by FIB was performed with a FEI Strata 400 DualBeam which was also used for the collection of the cross-sectional SEM images. The procedure requires the deposition of ~1.3 μm of platinum as the protection layer followed by FIB etching of ~5 μm. The images were collected at an angle of 52°. Film thickness was measured with a Filmetrics F20 Thin Film Measurement System and reported values are an average of 5 measurements over the entire surface with a deviation of ±5 nm. Silicon wafers were cleaned *via* a Harrick Scientific Corp. plasma cleaner/sterilizer (Model PDC-001) operating at ICP strength of 30 W and 100 mTorr of oxygen (O_2). A Phantom III ICP -RIE tool from Trion Technology Inc. was used for etching the NIL patterned substrates to generate free-standing nanostructures. Transmission electron microscopy (TEM) samples were prepared by scraping mesoporous silica from the substrate, grinding *via* mortar and pestle, suspended with ethanol and transferred to a holey-carbon-coated copper grid to be analyzed with a JEOL 2000FX II operating at 200 kV.

Results and discussion

To produce the desired hierarchical nanochannels, a six step approach was developed and is outlined in Fig. 1.

The process begins by making uniform thin films of UV curable monomers by spin-coating a solution of ~75 wt.% ethoxylated-bisphenol A dimethacrylate, ~23 wt.% trimethylolpropane triacrylate and ~2 wt.% 2,2-dimethoxy-2-phenylacetophenone dissolved in PGMEA onto a 3-(trimethoxysilyl) propyl methacrylate treated surface at 3000 rpm for 15 s in the presence of air. Typical concentrations ranged from 1 wt.% to 20 wt.% which yielded film thicknesses from ~25 nm to ~400 nm. The surface of the silicon wafer must be treated with 3-(trimethoxysilyl)propyl methacrylate to avoid dewetting of the UV curable monomer solution and to adjust the surface of the silicon wafer with a functionality that allows for participation in the crosslinking *via* UV exposure. To begin the fabrication of hierarchical silica nanochannels, an initial device level pattern consisting of a line array of ~650 nm wide, ~800 nm periodicity and ~200 nm tall lines was selected. To pattern the device level features, a thin film of ~90 nm from a 6 wt.% solution of the UV curable photopolymer was spin-coated at 3000 rpm for 15 s in the presence of air. UV assisted NIL was then performed with a transparent mold containing the device level features to create a replication of the mold into the UV curable photopolymer. For a detailed description of the mold fabrication, see Supporting Information, Schemes S1 and S2. Upon exposure to 365 nm UV light, the UV curable resist undergoes a crosslinking polymerization. A film thickness of ~90 nm yielded a minimal residual layer while achieving complete filling of the mold features. Swelling of the UV cured photopolymer was monitored in $scCO_2$ by variable angle spectroscopic ellipsometry (VASE) to check for pattern fidelity. It was determined that the UV cured photopolymer swelled a marginal amount of ~4% in the presence of $scCO_2$ at 125 bar and 60 °C. This minimal amount of swelling should not disrupt the dimensions of the polymer template.

Following NIL replication, the thin residual layer connecting the features was removed using dry etching. An ICP-RIE with O_2 plasma was applied resulted in free-standing structures. The plasma treatment resulted in a surface modification and yielded a more hydrophilic surface on the patterned silicon wafer. To monitor the depth of the O_2 plasma ICP-RIE etch, AFM was performed after each step and is detailed in Supporting Information, Fig. 3. The structure of the original NIL template ultimately dictates the dimensions of the embedded nanochannels and thus the device level feature of the hierarchical structure. After the O_2 plasma ICP-RIE etch, the line array dimensions were reduced to ~500 nm wide, ~750 nm periodicity and ~150 nm tall.

The amphiphilic block copolymers selected to template the domain level features (pores) are commercially available members of the BASF Pluronic® family. The Pluronic® family of block copolymer templates is based on triblock copolymers of poly(ethylene oxide)-*b*-poly(propylene oxide)-*b*-poly(ethylene oxide) [PEO-*b*-PPO-*b*-PEO]. Two triblock copolymers were chosen as templates from the Pluronic® series; Pluronic® F127,

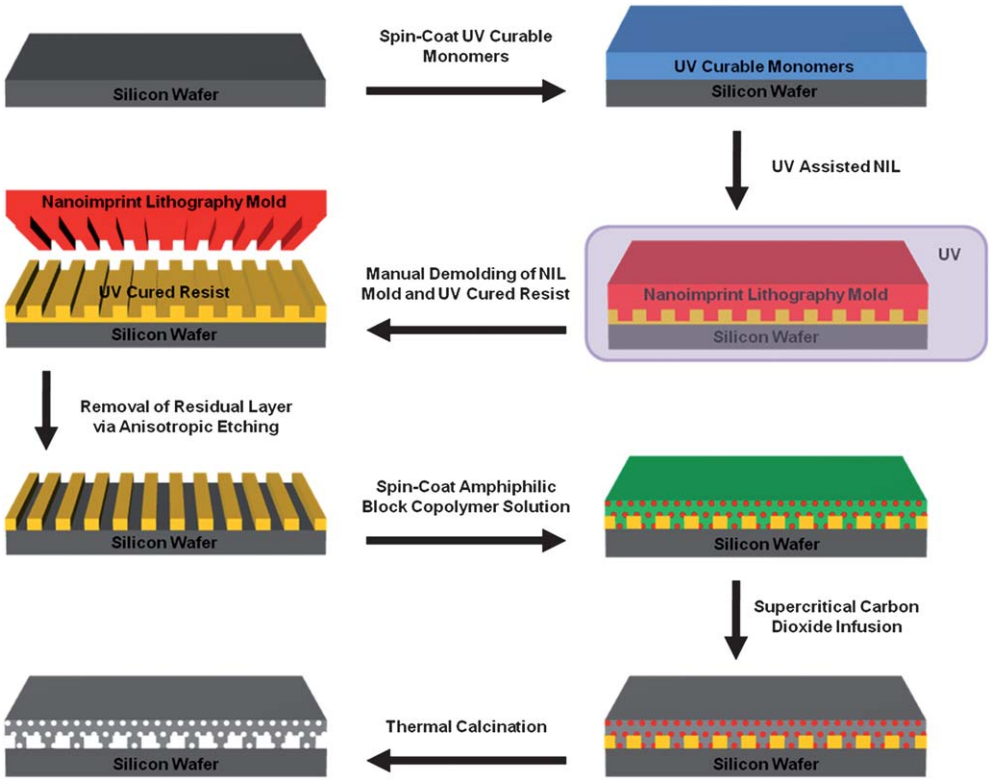

Fig. 1 Schematic showing the procedure to fabricate hierarchical silica nanostructures with domain and device level features.

PEO_{106}-*b*-PPO_{70}-*b*-PEO_{106}, which phase separates into a cylindrical morphology during the template process and Pluronic® F108, PEO_{127}-*b*-PPO_{48}-*b*-PEO_{127}, which phase separates into a spherical morphology. An organic acid catalyst, p-toluene sulfonic acid (pTSA), was added to the amphiphilic block copolymer solution to promote the hydrolysis and condensation of the silica network. The template also contains a hydrophilic homopolymer such as PAA or poly(4-hydroxystyrene) (PHOST) to help promote template phase segregation and long-range order of the domain level features.[30,31] A 10 wt.% solution of either Pluronic F127® or Pluronic F108® was prepared in a 50 : 50 ethanol:deionized (DI) water solution with 40 wt.% PAA (1.8k Mw, with respect to Pluronic F127® or Pluronic F108®) and 3 wt.% pTSA (with respect to solid material). The mixture was then directly spin-coated on the NIL patterned surface for 15 s at 3000 rpm forming a film of ~1 μm thick.

The next step was to transform the template into mesoporous silica. The block copolymer coated NIL template was exposed to a silicon alkoxide precursor, TEOS, solution in humidified $scCO_2$ at 60 °C and 125 bar for 2 h. Upon exposure to $scCO_2$, both the block copolymer template and the NIL template swell slightly allowing the TEOS to diffuse within both templates. As stated earlier, the acid catalyst, pTSA, selectively segregates to the hydrophilic segment of the block copolymer template within which hydrolysis and condensation of TEOS occurs. Little to no condensation of TEOS occurs within the hydrophobic segment of the block copolymer and the NIL template due to no acid catalyst being present. To ultimately form the hierarchical silica nanochannels, the polymer templates from both the block copolymer and NIL pattern are removed through thermal degradation. Accordingly, the substrates were heated at a 100 °C h^{-1} ramp rate from room temperature (RT) to 400 °C for 6 h and a ramp rate of 100 °C h^{-1} back to RT. TEM images of the domain level features for Pluronic® F127, Fig. 2a, and Pluronic® F108, Fig. 2b, templates show pore morphology of cylinders and spheres respectively with diameters of ~5–6 nm. To determine the fidelity of the device level feature focused ion beam scanning electron microscopy (FIB-SEM) was utilized.

Fig. 3 shows the image of the hierarchical silica nanochannels taken at an angle of 52° and the dimensions of the nanochannel are nearly identical to that of the polymer template prior to the $scCO_2$ infusion process.

The degradation of the polymer templates is of importance as to ensure that the nanochannel dimensions are transferred into the mesoporous silica with high accuracy and to avoid the nanochannel collapsing. To determine the thermal degradation

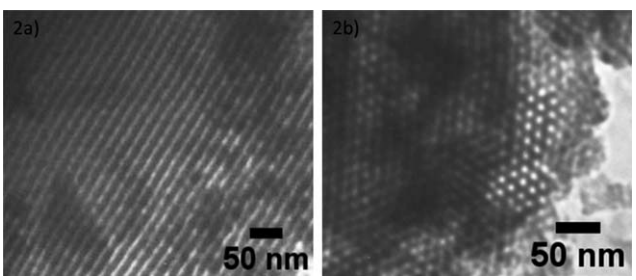

Fig. 2 Transmission electron micrographs showing the domain level features of the hierarchical silica nanochannel for a) Pluronic® F127, b) Pluronic® F108.

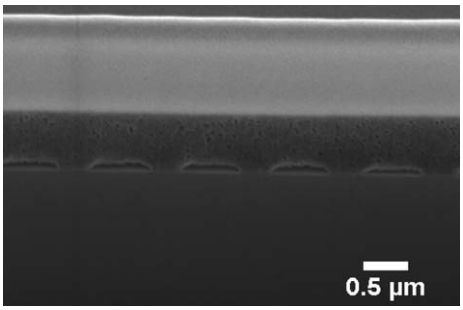

Fig. 3 Scanning electron micrograph showing the nanochannel dimension of the hierarchical silica nanochannel. Note that the defects visible in the silica film arise from the FIB sample preparation process and are considerably larger than the mesopores identified through TEM.

pathway of the polymer templates, thermogravimetric analysis (TGA) was performed and is provided in Fig. 4. From the TGA data, it was determined that the block copolymer template was removed first followed by the removal of the NIL template. This order of template removal provides highly accurate replication into the mesoporous silica due to the porosity imparted by the block copolymer template,[32] which provides a pathway for the degradation products of the NIL template to escape and yield crack-free films. To confirm the removal of polymeric templates from the hierarchical silica nanochannel, ATR-FT-IR was performed and the results are provided in Fig. 5. The TGA and ATR-FT-IR data confirm that the polymeric templates from both the block copolymer and NIL pattern were completely removed.

To demonstrate the utility of the hierarchical silica nanochannel structure, capacitance measurements were performed. The structure chosen for capacitance measurements was the metal-insulator-semiconductor (MIS) technique. Capacitance measurements were performed on device level features shown in Fig. 3 while the domain level features were synthesized using the Pluronic® F127 template with a silica precursor mixture of

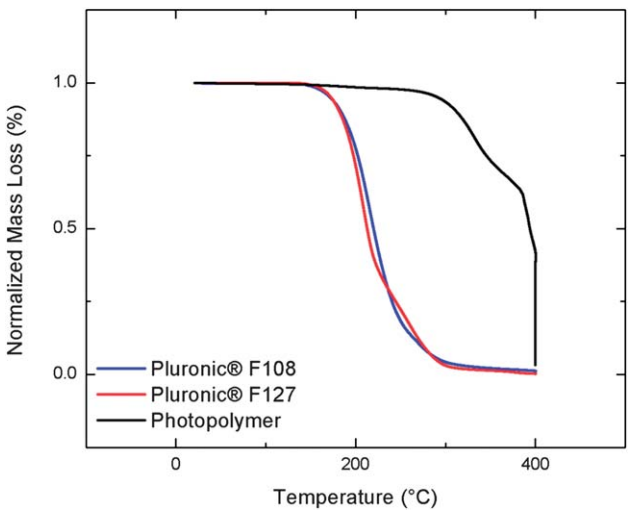

Fig. 4 Thermogravimetric analysis (TGA) of polymers templates: Pluronic® F108, F127 and photopolymer. TGA data shows that the polymer template directing domain level structure is degraded prior to the polymer template directing the device level structure.

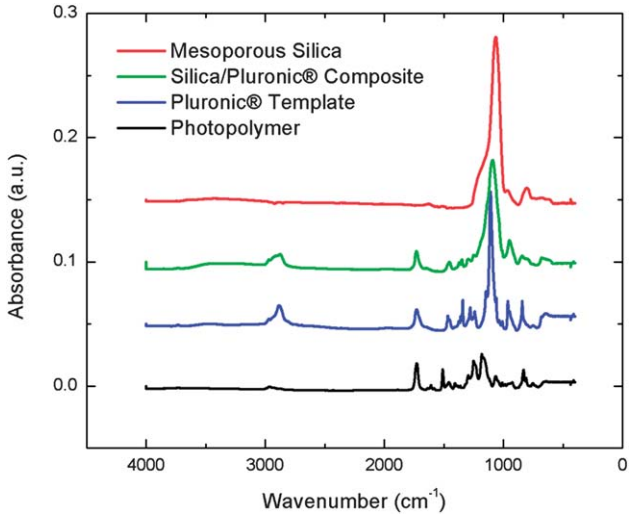

Fig. 5 ATR-FT-IR spectroscopy for the fabrication of hierarchical silica nanochannels.

60 : 40 TEOS:MTES (methyl triethoxysilane). The choice of this silica precursor introduces a hydrophobic methyl group into the silica matrix which makes the silica template more hydrophobic and less capable of absorbing water while providing the desired spherical morphology. The measurement of the non-air-gap sample yielded a dielectric constant of 2.1, which is in agreement with the value reported in the literature.[22] The air-gap sample yielded a dielectric constant of 2.0, which, based on the porosity and dimensions of the air-gap sample, is the theoretical value that was expected. It is recognized that the dimensions of the air-gap sample are not ideal for first level ILDs, however, this type of structure could be useful in the upper levels of the microprocessor architecture and active onboard cooling systems.

Conclusions

In summary, the combination of NIL and $scCO_2$ infusion allows for hierarchical silica nanochannels to be fabricated. The hierarchically structured silica nanochannels were investigated for use as a low-k dielectric material with a dielectric constant of 2.0 reported for channel dimensions of ~500 nm wide, ~750 nm periodicity and ~150 nm tall created by NIL. Domain level features with a diameter of ~5–6 nm of either spherical or cylindrical morphology were created by $scCO_2$ infusion. Domain level features, if desired, can be adjusted through modifications of the block copolymer template. The number of feature combinations that can be achieved are immense due to the availability of device level features afforded by NIL.

Acknowledgments

Funding for this research was provided by the National Science Foundation through the Center for Hierarchical Manufacturing (CHM, CMMI-0531171) at the UMass Amherst and a NIST/GRC Graduate Fellowship to N. R. Hendricks. FIB-SEM images were obtained from the Cornell Center for Materials Research (CCMR, DMR-0552782) with the assistance of Malcolm Thomas.

References

1 (*a*) J. L. Hedrick, R. D. Miller, C. J. Hawker, K. R. Carter, W. Volksen, D. Y. Yoon and M. Trollsås, *Adv. Mater.*, 1998, **10**, 1049–1053; (*b*) C. V. Nguyen, K. R. Carter, C. J. Hawker, J. L. Hedrick, R. L. Jaffe, R. D. Miller, J. F. Remenar, H. W. Rhee, P. M. Rice, M. F. Toney, M. Trollsas and D. Y. Yoon, *Chem. Mater.*, 1999, **11**(11), 3080–3085.

2 S. Baskaran, J. Liu, K. Domansky, N. Kohler, X. Li, C. Coyle, G. E. Fryxell, S. Thevuthasan and R. E. Williford, *Adv. Mater.*, 2000, **12**, 291–294.

3 G. Wirnsberger, P. Yang, B. J. Scott, B. F. Chmelka and G. D. Stucky, *Spectrochim. Acta, Part A*, 2001, **57**, 2049–60.

4 A. Corma, *Chem. Rev.*, 1997, **97**, 2373–2420.

5 A. Stein, *Adv. Mater.*, 2003, **15**, 763–775.

6 P. Innocenzi, *Sens. Actuators, B*, 2001, **76**, 299–303.

7 P. Innocenzi, A. Martucci, M. Guglielmi, A. Bearzotti, E. Traversa and J. C. Pivin, *J. Eur. Ceram. Soc.*, 2001, **21**, 1985–1988.

8 H.-T. Chen, T. a. Crosby, M.-H. Park, S. Nagarajan, V. M. Rotello and J. J. Watkins, *J. Mater. Chem.*, 2009, **19**, 70.

9 H. Seidel, *J. Electrochem. Soc.*, 1990, **137**, 3612.

10 H. Seidel, *J. Electrochem. Soc.*, 1990, **137**, 3612.

11 W. Li, J. O. Tegenfeldt, L. Chen, R. H. Austin, S. Y. Chou, P. a. Kohl, J. Krotine and J. C. Sturm, *Nanotechnology*, 2003, **14**, 578–583.

12 D. Xia, T. C. Gamble, E. A. Mendoza, S. J. Koch, X. He, G. P. Lopez and S. R. J. Brueck, *Nano Lett.*, 2008, **8**, 1610–8.

13 H. Cao, Z. Yu, J. Wang, J. O. Tegenfeldt, R. H. Austin, E. Chen, W. Wu and S. Y. Chou, *Appl. Phys. Lett.*, 2002, **81**, 174–176.

14 L. J. Guo, X. Cheng and C.-F. Chou, *Nano Lett.*, 2004, **4**, 69–73.

15 X. Liang, K. J. Morton, R. H. Austin and S. Y. Chou, *Nano Lett.*, 2007, **7**, 3774–80.

16 J. R. Ell, T. a. Crosby, J. J. Peterson, K. R. Carter and J. J. Watkins, *Chem. Mater.*, 2010, **22**, 1445–1451.

17 M. J. De Boer, R. W. Tjerkstra, J. W. Berenschot, H. V. Jansen, G. J. Burger, J. G. E. Gardeniers, M. Elwenspoek and a van den Berg, *J. Microelectromech. Syst.*, 2000, **9**, 94–103.

18 J. L. Perry and S. G. Kandlikar, *Microfluid. Nanofluid.*, 2005, **2**, 185–193.

19 M. Pantouvaki, A. Humbert, E. Vanbesien, E. Camerotto, Y. Travaly, O. Richard, M. Willegems, H. Volders, K. Kellens and R. Daamen, *Microelectron. Eng.*, 2008, **85**, 2071–2074.

20 R. Hoofman, R. Caluwaerts, J. Michelon, P. Herrerobernabe, J. Gueneaudemussy, C. Bruynseraede, J. Lee, S. List, P. Bancken and G. Beyer, *Microelectron. Eng.*, 2006, **83**, 2150–2154.

21 J. Noguchi, K. Sato, N. Konishi, S. Uno, T. Oshima, K. Ishikawa, H. Ashihara, T. Saito, M. Kubo, T. Tamaru, Y. Yamada, H. Aoki and T. Fujiwara, *IEEE Trans. Electron Devices*, 2005, **52**, 352–359.

22 R. A. Pai, R. Humayun, M. T. Schulberg, A. Sengupta, J.-N. Sun and J. J. Watkins, *Science*, 2004, **303**, 507–510.

23 S. Nagarajan, M. Li, R. a. Pai, J. K. Bosworth, P. Busch, D.-M. Smilgies, C. K. Ober, T. P. Russell and J. J. Watkins, *Adv. Mater.*, 2008, **20**, 246–251.

24 S. Nagarajan, J. K. Bosworth, C. K. Ober, T. P. Russell and J. J. Watkins, *Chem. Mater.*, 2008, **20**, 604–606.

25 A. H. Romang and J. J. Watkins, *Chem. Rev.*, 2010, **110**, 459–478.

26 S. Y. Chou, P. R. Krauss and P. J. Renstrom, *Appl. Phys. Lett.*, 1995, **67**, 3114–3116.

27 L. J. Guo, *Adv. Mater.*, 2007, **19**, 495–513.

28 J. Haisma, M. Verheijen, K. van den Heuvel and J. van den Berg, *J. Vac. Sci. Technol., B*, 1996, **14**, 4124–4128.

29 B. D. Gates, Q. Xu, M. Stewart, D. Ryan, C. G. Willson and G. M. Whitesides, *Chem. Rev.*, 2005, **105**, 1171–1196.

30 V. R. Tirumala, R. a. Pai, S. Agarwal, J. J. Testa, G. Bhatnagar, A. H. Romang, C. Chandler, B. P. Gorman, R. L. Jones, E. K. Lin and J. J. Watkins, *Chem. Mater.*, 2007, **19**, 5868–5874.

31 V. R. Tirumala, A. Romang, S. Agarwal, E. K. Lin and J. J. Watkins, *Adv. Mater.*, 2008, **20**, 1603–1608.

32 B. D. Vogt, R. a. Pai, H.-J. Lee, R. C. Hedden, C. L. Soles, W.-li Wu, E. K. Lin, B. J. Bauer and J. J. Watkins, *Chem. Mater.*, 2005, **17**, 1398–1408.

